

Dark-Field Imaging on a Clinical CT System: Realization of Talbot-Lau Interferometry in a Gantry

Manuel Viermetz^{a,b}, Nikolai Gustschin^{a,b}, Clemens Schmid^{a,b}, Jakob Haeusele^{a,b},
Roland Proksa^c, Thomas Koehler^{c,d}, and Franz Pfeiffer^{a,b,d,e}

^aChair of Biomedical Physics, Department of Physics, Technical University of Munich, 85748
Garching, Germany

^bMunich Institute of Biomedical Engineering, Technical University of Munich, 85748 Garching,
Germany

^cPhilips Research, 22335 Hamburg, Germany

^dInstitute for Advanced Study, Technical University of Munich, 85748 Garching, Germany

^eDepartment of Diagnostic and Interventional Radiology, School of Medicine and Klinikum
rechts der Isar, Technical University of Munich, 81675 Munich, Germany

ABSTRACT

Computed tomography (CT) is a foundation of modern clinical diagnostics but it presently only retrieves information from X-rays attenuation. However, it is known that micro structural texture or porosity – which is well below the spatial resolution of CT – can be revealed by grating-based dark-field imaging. Diagnostic value of this sub-resolution tissue information has been demonstrated in pre-clinical studies on small-animal disease models and recently also in a first clinical radiography system.¹ These studies show that dark-field imaging is particularly useful for early detection and staging of lung diseases.

While dark-field CT is regularly realized in laboratory environment, the transfer to human scale and bringing it to clinical application poses several technical challenges. Switching from a step-and-shoot acquisition to a mode where the gantry and acquisition operate continuously as well as reducing scan times to below seconds and ensuring stability against vibrations are key concerns when it comes to the translation of the established laboratory dark-field technology to full-body medical CT. In,² we recently demonstrated the first dark-field CT implementation, which collectively solves these roadblocks and therefore is a milestone in the development of clinical CT imaging. The prototype we present allows to reconstruct the attenuation and dark-field channels of a human thorax phantom from a one second long acquisition and covers a 45 cm diameter field of view.

In this work, we present how the first dark-field CT prototype works and focus particularly on the technical design, optimized design of the gratings for CT application and the first characterization of the interferometer in the rotating gantry. We discuss which steps were particularly important for the realization and where we see potential for further improvements. These results provide key insights for future dark-field CT implementations.

Keywords: X-ray Imaging, Dark-field contrast, Computed Tomography, Talbot-Lau interferometer

1. INTRODUCTION

X-ray Computed Tomography (CT) is a well-established technique, which is – in its conventional form – limited to attenuation contrast. There it allows high resolution imaging, fast acquisition times, and decent contrast for many purposes such as material research, inspection, and medical diagnostics. Throughout the last decade Talbot-Lau interferometry, which started as a synchrotron-only technology, gained attention as it unlocks additional contrast channels.^{3,4} A Talbot-Lau interferometer, as illustrated in Fig. 1, allows simultaneous imaging of attenuation, refraction, and small-angle scattering of the transmitted object.^{5,6}

Send correspondence to Manuel Viermetz (contact.viermetz@tum.de)

Particularly the access to sub-resolution tissue properties by analyzing the small-angle scattering power – also referred to as dark-field signal – of the material is a promising application in biomedical imaging. Previous work at laboratory setups demonstrated that the dark-field modality is useful for lung diagnostics as it enables the detection of micro-structural changes in lung parenchyma.^{7–10}

Recently the first clinical study on dark-field chest radiography of COPD and COVID-19 patients validated these pre-clinical results and clearly showed the potential of this additional image contrast.^{1,11} This first in-vivo human dark-field imaging system can now retrieve otherwise undetectable changes in the porous lung tissue which are correlated with diseases progressions. However, this chest radiography provides no 3D information and anatomical structures overlap in image domain. To overcome these restrictions our approach is to install the interferometer into a clinical CT gantry. However, this step involves a variety of problems since the space on a clinical CT gantry is limited, an extremely large field of view must be covered by the gratings (compared to current state of the art dark-field implementations), and vibrations of the system can quickly degrade the measured signal. In this work we discuss our design of a Talbot-Lau interferometer which has been integrated into a Brilliance iCT (Royal Philips, The Netherlands) and produces the first dark-field CT reconstructions of human sized phantoms.²

2. TALBOT-LAU INTERFEROMETER LAYOUT

In our presented design the most important design rules have been (1) to maintain the bore diameter of the conventional CT, which is 70 cm (blue dashed line in Fig. 1), (2) to not modify the conventional gantry and its primary imaging components, i.e., source and detector, and (3) to have at least 45 cm coverage which is 90% of a conventional CT which has an diameter of 50 cm (highlighted area and green dashed line in Fig. 1, respectively).

The presented Talbot-Lau interferometer consists of three gratings and must be optimized for the 80 kVp spectrum, which is the lowest available energy on the iCT platform. As this method only works for coherent

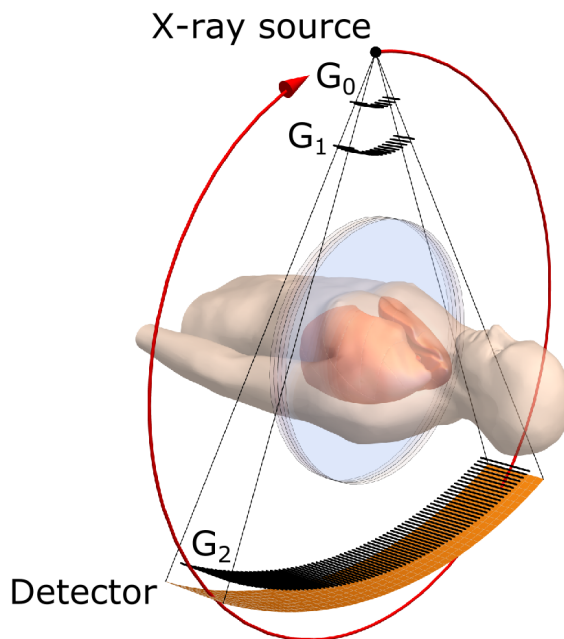


Figure 1. Talbot-Lau interferometer in a CT gantry. It consists of three cylindrically bent gratings illustrated as line patterns, referred to as G_0 , G_1 , and G_2 , which structure the X-ray beam as they absorb or phase-shift the radiation. By the Talbot effect a self-image of G_1 appears at the location of G_2 . The object induces attenuation, refraction, and small-angle scattering, which subsequently change this self-image characteristically. Using the Moiré effect and the G_2 grating which has a period matching to the G_1 self-image these distortions can be retrieved with a common X-ray detector. Since this approach relies on coherent radiation, a G_0 source-grating is required to convert the incoherent source spot into a set of sufficiently coherent slit sources.

radiation a source grating G_0 is required.¹² It splits the radiation from the incoherent X-ray source into several slit sources which fulfill the coherence requirement for the length of the interferometer setup. Because of the weak interaction between hard X-rays and grating the aspect ratio of the structures must be high – which is difficult to fabricate – and gold as a good absorber is used as the grating material. The grating G_1 introduces a fine intensity modulation on the incident radiation, which is basically a fine line pattern with a periodicity of a few micrometers. Attenuation of the radiation by the object causes a decrease of intensity, whereas refraction and small-angle scattering induce small distortions of the pattern. To resolve these small changes an analyzer grating G_2 is positioned in front of the detector and makes use of the Moiré effect to translate the changes to an intensity pattern which can be measured by the detector.

The grating periods and distances define the sensitivity of the system to small-angle scattering. Basically, smaller periods and longer distances lead to a more sensitive setup. Note that a too small sensitivity results in a poor signal to noise ratio and a too high sensitivity can lead to artefacts due visibility starvation. From previous work in^{13,14} a sensitivity range that is meaningful for lung imaging can be derived. To achieve a sufficient sensitivity the position and the period of the grating structures must be selected carefully. Certainly higher sensitivity is preferred, however, there are limitations in the grating fabrication and the available space on the CT gantry which limit the maximum sensitivity of our prototype.

In Fig. 2 two sketches of different geometries illustrate possible implementations of the three gratings into a CT gantry. Increasing inter-grating distances as well as decreasing the grating periods improve sensitivity. Evidently, it is therefore a good design choice to maximize the distances within the constraints given by the CT platform.¹⁵ Consequently G_0 and G_2 are positioned as close to the X-ray source and the detector, respectively, and G_1 as close to the bore as possible. The inverse geometry is advantageous for our CT implementation as it requires only one large coverage G_2 with relatively coarse period and the gratings G_0 and G_1 are small enough to be manufactured as single parts.

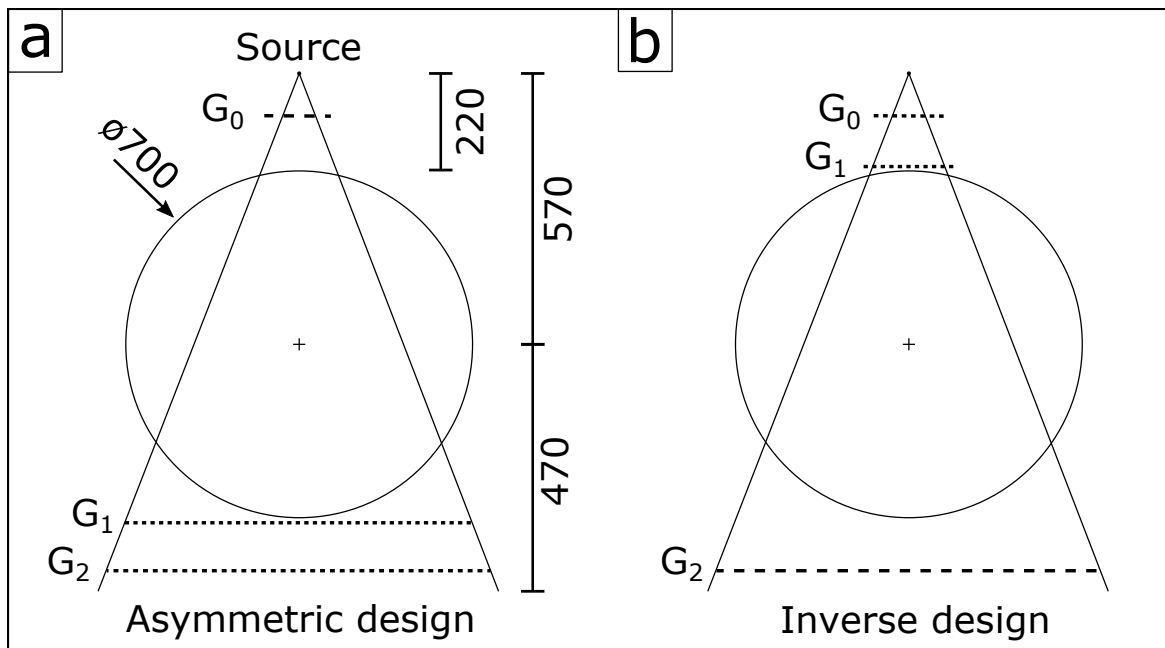


Figure 2. Asymmetric and inverse interferometer geometry. **a**, in an asymmetric design the gratings G_1 and G_2 are both behind the patient and must cover a large area due to the large field of view. Furthermore, the periods of these two gratings are rather fine, compared to the G_0 grating. **b**, in the inverse geometry, G_0 and G_1 are in front of the patient, their size is relatively small due to the strong divergence of the setup, and the period of the largest grating G_2 is coarse, which makes fabrication easier. Another advantage of this design is its dose efficiency because G_1 is positioned in front of the patient.

3. INTEGRATION INTO THE CT GANTRY

In our implementation we position a combined mount which holds G_0 and G_1 into the collimator box which is positioned downstream the X-ray source before the patient. This assembly is shown in Fig. 3 where the two gratings are cylindrically bent to focus towards the X-ray source spot of the CT. This is an important design characteristic since grating G_0 exceeds an aspect ratio of 100 (relation between height and width of the lamellae). In an un-bent state, a significant fraction of the radiation would traverse the grating not with a perpendicular incident angle because of the strong divergence. This would lead to a degradation of the slit-sources by shadowing, which should be generated by the G_0 , and consequently the performance of the interferometer vanishes.

The large G_2 grating must cover about 80 cm of arc length which is realized by combining several smaller tiles to one large grating. We developed a specialized mount which allows us to adjust the tiles inside the gantry individually and which additionally bends each tile to focus towards the source spot. It is shown in Fig. 4 covering 90% of the CT detector columns and 32 pixel rows which leads to a total coverage of 20 mm in the iso-center and a reconstructible volume diameter of 450 mm.

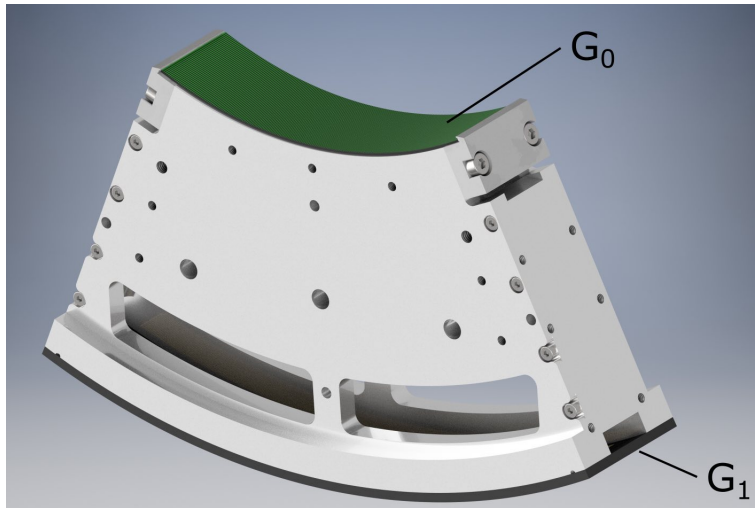


Figure 3. G_0 and G_1 bending frame for CT implementation. The two gratings are rigidly mounted on a machined structure which ensures a precise inter-grating distance and bends the gratings cylindrically. This focuses the trenches between the grating lamellae towards the X-ray source spot to compensate for the strongly divergent radiation and reduce shadowing artefacts.

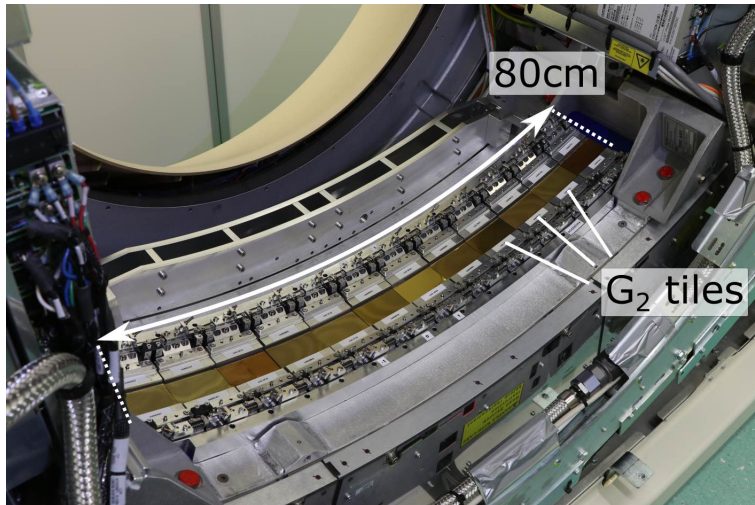


Figure 4. Modular G_2 implementation covering 80 cm width. The specialized mount allows adjustment of each G_2 tiles individually to minimize the gap between the tiles and to ensure parallel alignment of the G_2 lamellae to the line pattern produced by the G_1 . Again, each grating tile is bent cylindrically and also the combined assembly follows this curvature to focus into the source spot, which reduces shadowing artefacts.

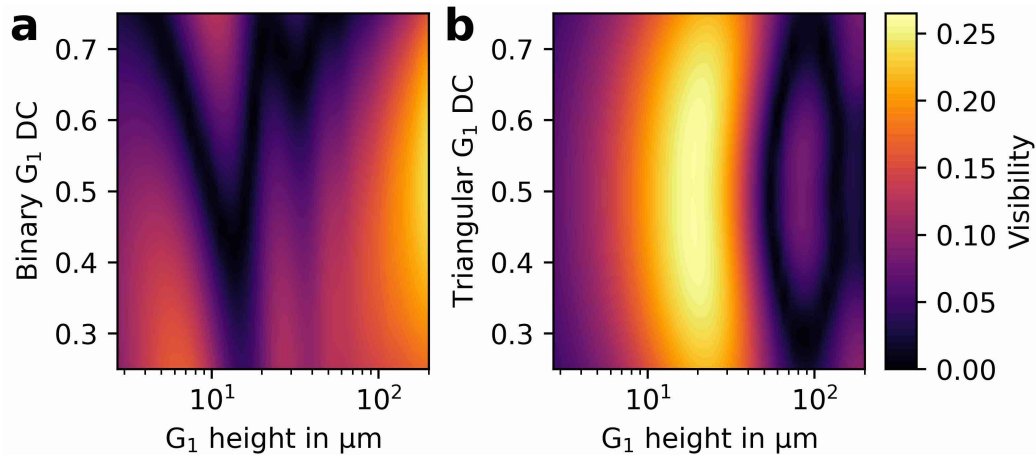


Figure 5. Wave optical simulation results of the interferometer for different G_1 parameters (using gold as a grating material). **a**, shows the performance for a conventional Talbot-Lau interferometer with rectangular or binary grating profile. Here we find no significant performance in the height range typical for phase-shifting G_1 (below $25\ \mu\text{m}$) merely a design with an absorption G_1 (height exceeding $200\ \mu\text{m}$) would give good performance. **b**, only for a triangular G_1 grating profile with a height of $18\ \mu\text{m}$ a good performance exceeding 26% visibility is found.

4. OPTIMIZATION OF THE GRATING PARAMETERS

Based on the state of the art fabrication technology for X-ray absorption gratings, which are compatible with the 80 kVp spectrum used in our dark-field CT prototype and a ballpark sensitivity estimation that shows that we will not reach the upper sensitivity limit for human lung imaging where signal saturation occurs, the period of G_0 is fixed to $4.8\ \mu\text{m}$. From this parameter and the introduced inverse interferometer geometry we derive the optimal grating parameters using a wave propagation simulation. It is similar to previous work by¹⁶ and includes the geometrical effects of the diverging beam, the selected X-ray source spot, the clinical 80 kVp spectrum, its filtration, and the imperfections in the extended gratings, i.e. bridges in the layout.

Apart from the sensitivity (which is defined by distances and periods), another key parameter of the interferometer is the so-called fringe visibility, which directly translates into signal to noise ratio of the dark-field image.¹⁷ This visibility is strongly influenced by the height, shape, and duty cycle of the grating G_1 . In Fig. 5 simulation results of these free parameters reveal significant performance differences, particularly for two different G_1 grating profiles. We find that the best system performance can be achieved with a triangular shaped G_1 grating profile.¹⁸ The elegance of a triangular G_1 profile is that it requires only about $18\ \mu\text{m}$ high structures and thus, X-ray flux through this grating remains high whereas the alternative – an absorption G_1 – would reduce the flux at least by 50%. Furthermore, an absorption G_1 would require a high aspect ratio which makes its fabrication difficult.

The dark-field CT prototype is equipped with a triangular G_1 on a flexible polyimide substrate. The flexibility of the substrate enables us to bend the structure as discussed earlier and ensures that the performance is not degraded, e.g. by scattering of radiation in the substrate material. G_0 and G_2 use graphite substrates which are also flexible for bending to the required radii.

5. PERFORMANCE OF THE TALBOT-LAU INTERFEROMETER

The design utilizes the standard iCT detector and can be rotated with rotation times between 0.27 and 1.5 s which are the standard settings for this clinical CT model. From the centrifugal acceleration and the vibrations induced by the X-ray tube as well as other sources of instabilities the interferometer is periodically leading to a corresponding distortion of the fringe pattern.. Fortunately, the frame rate of the detector is high enough to resolve the distortions with high accuracy, thus, with a sophisticated processing framework the attenuation and dark-field signal can be extracted from the measurements.

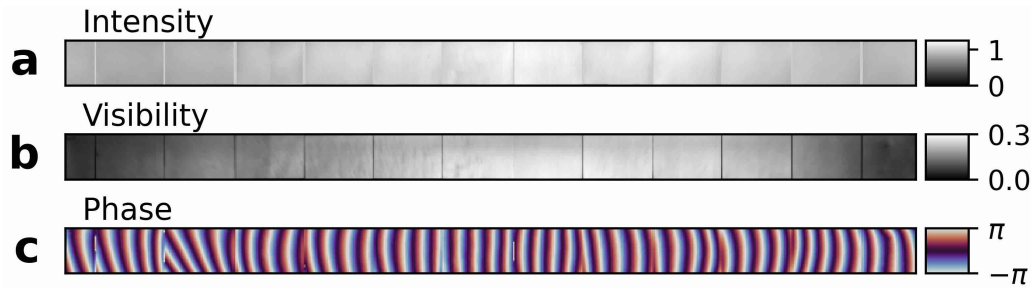


Figure 6. Performance evaluation of the Talbot-Lau interferometer during rotation. **a**, the intensity has a characteristic maximum in the center and decreases to the left and right due to partial shadowing in the G_0 . **b**, the system visibility is highest in the center exceeding 26%, but due to partial shadowing there is a drop to the left and right. **c**, the interferometer phase is optimized for about 10 pixels per fringe for ideal phase sampling during processing and reconstruction.

The visibility of the presented interferometer, which is the most important measure for the performance of a Talbot-Lau interferometer, is around 22% for the central 50% of the field of view. Fig. 6 shows the flat-field performance of the interferometer where a characteristic reduction towards the left and right is induced by remaining partial shadowing in G_0 due to the large source spot. For larger fan angles, the width of the X-ray source spot appears to be bigger, because the actual source area is an inclined plane on the anode target surface. Only under the projection through the iso-centre the source spot is smallest.

6. CONCLUSION

We conclude that the presented design is most suitable for clinical dark-field CT implementation within the limitations of current grating fabrication and the geometrical boundary conditions imposed by the desire to use a conventional clinical CT as a platform for the prototype. We analyzed the impact of the most important design parameters to identify potential problems and could verify that a triangular grating profile for G_1 has the best performance, besides an absorption G_1 .

In our implementation shadowing is avoided by cylindrically bending all gratings to focus into the source spot. Nevertheless, partial shadowing in the G_0 due to the extended source causes a visibility decrease towards larger fan-angles.

With this proposed design, we demonstrate that implementation of a Talbot-Lau interferometer into a clinical CT is feasible with state of the art gratings. This development now brings dark-field CT an important step closer to the clinics as it demonstrates that up-scaling to human sized field of views works and sub-second scan times are now easily possible.

ACKNOWLEDGMENTS

The authors wish to thank Julia Herzen, Daniela Pfeiffer, Alexander Fingerle, Ernst Rummeny, Pascal Meyer, Jürgen Mohr, Maximilian von Teuffenbach, Amanda Pleier, Michael Heider, Sven Prevrhal, Thomas Reichel, Stefan Löscher, Frank Bergner, Ami Altman, and Shlomo Gotman for their help, support, and dedication to launch this complex project. This work was carried out with the support of the Karlsruhe Nano Micro Facility (KNMF, www.kit.edu/knmf), a Helmholtz Research Infrastructure at Karlsruhe Institute of Technology (KIT). We acknowledge the support of the TUM Institute for Advanced Study, funded by the German Excellence Initiative, the European Research Council (ERC, H2020, AdG 695045) and Philips GmbH Market DACH.

REFERENCES

- [1] Willer, K., Fingerle, A. A., Noichl, W., De Marco, F., Frank, M., Urban, T., Schick, R., Gustschin, A., Gleich, B., Herzen, J., Koehler, T., Yaroshenko, A., Pralow, T., Zimmermann, G. S., Renger, B., Sauter, A. P., Pfeiffer, D., Makowski, M. R., Rummeny, E. J., Grenier, P. A., and Pfeiffer, F., "X-ray dark-field chest imaging for detection and quantification of emphysema in patients with chronic obstructive pulmonary disease: a diagnostic accuracy study," *The Lancet Digital Health* **3**, e733–e744 (Nov. 2021).

- [2] Viermetz, M., Gustschin, N., Schmid, C., Haeusele, J., von Teuffenbach, M., Meyer, P., Bergner, F., Lasser, T., Proksa, R., Koehler, T., and Pfeiffer, F., “Dark-field computed tomography reaches the human scale,” *Proceedings of the National Academy of Sciences* **119**(8), e2118799119 (2022).
- [3] Pfeiffer, F., Weitkamp, T., Bunk, O., and David, C., “Phase retrieval and differential phase-contrast imaging with low-brilliance x-ray sources,” *Nature Physics* **2**, 258–261 (4 2006).
- [4] Weitkamp, T., David, C., Kottler, C., Bunk, O., and Pfeiffer, F., “Tomography with grating interferometers at low-brilliance sources,” 249 – 258, International Society for Optics and Photonics, SPIE (2006).
- [5] Pfeiffer, F., Bech, M., Bunk, O., Kraft, P., Eikenberry, E. F., BrÖnnimann, C., Grünzweig, C., and David, C., “Hard-x-ray dark-field imaging using a grating interferometer,” *Nature Materials* **7**, 134–137 (2 2008).
- [6] Bech, M., Bunk, O., Donath, T., Feidenhans'l, R., David, C., and Pfeiffer, F., “Quantitative x-ray dark-field computed tomography,” *Physics in Medicine and Biology* **55**, 5529–5539 (9 2010).
- [7] Meinel, F. G., Yaroshenko, A., Hellbach, K., Bech, M., Müller, M., Velroyen, A., Bamberg, F., Eickelberg, O., Nikolaou, K., Reiser, M. F., Pfeiffer, F., and Yildirim, A. Ö., “Improved diagnosis of pulmonary emphysema using in vivo dark-field radiography,” *Investigative Radiology* **49**(10) (2014).
- [8] Hellbach, K., Yaroshenko, A., Meinel, F. G., Yildirim, A. O., Conlon, T. M., Bech, M., Mueller, M., Velroyen, A., Notohamiprodjo, M., Bamberg, F., Auweter, S., Reiser, M., Eickelberg, O., and Pfeiffer, F., “In vivo dark-field radiography for early diagnosis and staging of pulmonary emphysema,” *Invest Radiol* **50** (2015).
- [9] Velroyen, A., Yaroshenko, A., Hahn, D., Fehringer, A., Tapfer, A., Müller, M., Noël, P. B., Pauwels, B., Sasov, A., Yildirim, A., Eickelberg, O., Hellbach, K., Auweter, S. D., Meinel, F. G., Reiser, M. F., Bech, M., and Pfeiffer, F., “Grating-based x-ray dark-field computed tomography of living mice,” *EBioMedicine* **2**, 1500–1506 (10 2015).
- [10] Modregger, P., Cremona, T. P., Benarafa, C., Schittny, J. C., Olivo, A., and Endrizzi, M., “Small angle x-ray scattering with edge-illumination,” *Scientific Reports* **6** (Nov. 2016).
- [11] Frank, M., Gassert, F., Urban, T., Willer, K., Noichl, W., Schick, R., Schultheiss, M., Viermetz, M., Gleich, B., De Marco, F., Herzen, J., Koehler, T., Engel, K.-J., Renger, B., Gassert, F., Sauter, A., Fingerle, A., Haller, B., Makowski, M., Pfeiffer, D., and Pfeiffer, F., “Dark-field Chest X-ray Imaging for the Assessment of COVID-19-Pneumonia,” *submitted* .
- [12] Pfeiffer, F., Kottler, C., Bunk, O., and David, C., “Hard x-ray phase tomography with low-brilliance sources,” *Physical Review Letters* **98**, 108105 (3 2007).
- [13] Yashiro, W., Terui, Y., Kawabata, K., and Momose, A., “On the origin of visibility contrast in x-ray Talbot interferometry,” *Optics Express* **18**, 16890 (Aug. 2010). ISBN: 1094-4087.
- [14] Ludwig, V., Seifert, M., Hauke, C., Hellbach, K., Horn, F., Pelzer, G., Radicke, M., Rieger, J., Sutter, S. M., Michel, T., and Anton, G., “Exploration of different x-ray Talbot-Lau setups for dark-field lung imaging examined in a porcine lung,” *Physics in Medicine and Biology* **64** (2019).
- [15] Donath, T., Chabior, M., Pfeiffer, F., Bunk, O., Reznikova, E., Mohr, J., Hempel, E., Popescu, S., Hoheisel, M., Schuster, M., Baumann, J., and David, C., “Inverse geometry for grating-based x-ray phase-contrast imaging,” *Journal of Applied Physics* **106** (2009).
- [16] Ritter, A., Bartl, P., Bayer, F., Gödel, K. C., Haas, W., Michel, T., Pelzer, G., Rieger, J., Weber, T., Zang, A., and Anton, G., “Simulation framework for coherent and incoherent X-ray imaging and its application in Talbot-Lau dark-field imaging,” *Optics Express* **22**, 23276 (Sept. 2014). Publisher: The Optical Society.
- [17] Weber, T., Bartl, P., Bayer, F., Durst, J., Haas, W., Michel, T., Ritter, A., and Anton, G., “Noise in x-ray grating-based phase-contrast imaging,” *Medical Physics* **38**, 4133–4140 (2011).
- [18] Yaroshenko, A., Malecki, A., Tapfer, A., Kunka, D., Pfeiffer, F., Potdevin, G., Meiser, J., Wolf, J., Mohr, J., Schüttler, M., Bech, M., Amberger, M., and Biernath, T., “Non-binary phase gratings for x-ray imaging with a compact Talbot interferometer,” *Optics Express* **22**, 547–556 (1 2014).